Sensing with magnetic dipolar resonances in semiconductor nanospheres

Braulio García-Cámara,[1,2,4] Raquel Gómez-Medina,[5] Juan José Sáenz,[5] and Borja Sepúlveda[1,2,3,*]

[1]*ICN2 –Institut Catala de Nanociencia i Nanotecnologia, Campus UAB, 08193 Bellaterra (Barcelona), Spain*
[2]*CSIC - Consejo Superior de Investigaciones Científicas, ICN2 Building, 08193Bellaterra (Barcelona), Spain*
[3]*CIBER-BBN, Spain*
[4]*Department of Electronic Technology, Carlos III University of Madrid, Av. de la Universidad s/n, 28911 Leganés, Madrid, Spain*
[5]*Departamento de Física de la Materia Condensada, Instituto"Nicolás Cabrera" and Centro de Investigación en Física de la Materia Condensada (IFIMAC).Universidad Autónoma de Madrid. Campus de Cantoblanco, 28049, Madrid, Spain*
[*]*borja.sepulveda@cin2.es*

Abstract: In this work we propose two novel sensing principles of detection that exploit the magnetic dipolar Mie resonance in high-refractive-index dielectric nanospheres. In particular, we theoretically investigate the spectral evolution of the extinction and scattering cross sections of these nanospheres as a function of the refractive index of the external medium (n_{ext}). Unlike resonances in plasmonic nanospheres, the spectral position of magnetic resonances in high-refractive-index nanospheres barely shifts as n_{ext} changes. Nevertheless, there is a drastic reduction in the extinction cross section of the nanospheres when n_{ext} increases, especially in the magnetic dipolar spectral region, which is accompanied with remarkable variations in the radiation patterns. Thanks to these changes, we propose two new sensing parameters, which are based on the detection of: i) the intensity variations in the transmitted or backscattered radiation by the dielectric nanospheres at the magnetic dipole resonant frequency, and ii) the changes in the radiation pattern at the frequency that satisfies Kerker's condition of near-zero forward radiation. To optimize the sensitivity, we consider several semiconductor materials and particles sizes.

OCIS codes: (300.6470) Spectroscopy, semiconductors; (280.4788) Optical sensing and sensors.

References and links

1. V. R. Almeida, C. A. Barrios, R. R. Panepucci, and M. Lipson, "All-optical control of light on a silicon chip," Nature **431**(7012), 1081–1084 (2004).
2. H. Rong, A. Liu, R. Jones, O. Cohen, D. Hak, R. Nicolaescu, A. Fang, and M. Paniccia, "An all-silicon Raman laser," Nature **433**(7023), 292–294 (2005).
3. G. T. Reed, *Silicon Photonics: The State of Art* (John Wiley & Sons, 2008).
4. K. Zinoviev, L. G. Carrascosa, J. Sánchez del Río, B. Sepúlveda, C. Domínguez, and L. M. Lechuga, "Silicon photonic biosensors for lab-on-a-chip applications," Adv. Opt. Technol. **2008**, 383927 (2008).
5. A. Densmore, M. Vachon, D.-X. Xu, S. Janz, R. Ma, Y.-H. Li, G. Lopinski, A. Delâge, J. Lapointe, C. C. Luebbert, Q. Y. Liu, P. Cheben, and J. H. Schmid, "Silicon photonic wire biosensor array for multiplexed real-time and label-free molecular detection," Opt. Lett. **34**(23), 3598–3600 (2009).
6. M. Ibisate, D. Golmayo, and C. López, "Silicon direct opals," Adv. Mater. **21**(28), 2899–2902 (2009).
7. N. Sherwood-Droz, A. Gondarenko, and M. Lipson, "Oxidized silicon-on-insulator (OxSOI) from bulk silicon: a new photonic platform," Opt. Express **18**(6), 5785–5790 (2010).
8. A. C. Turner-Foster, M. A. Foster, J. S. Levy, C. B. Poitras, R. Salem, A. L. Gaeta, and M. Lipson, "Ultrashort free-carrier lifetime in low-loss silicon nanowaveguides," Opt. Express **18**(4), 3582–3591 (2010).
9. B. García-Cámara, *Communication Architectures for Systems on Chip* (Taylor and Francis, 2011), pp.249–322.
10. M. A. Pannicia, "Perfect marriage: optics and silicon," Optik Photonik **6**, 34–38 (2011).

#189057 - $15.00 USD Received 17 Apr 2013; revised 26 Jun 2013; accepted 31 Jul 2013; published 23 Sep 2013

11. L. Shi, T. U. Tuzer, R. Fenollosa, and F. Meseguer, "A new dielectric metamaterial building block with a strong magnetic response in the sub-1.5-micrometer region: silicon colloid nanocavities," Adv. Mater. **24**(44), 5934–5938 (2012).
12. J. Xia, A. M. Rossi, and T. E. Murphy, "Laser-written nanoporous silicon ridge waveguide for highly sensitive optical sensors," Opt. Lett. **37**(2), 256–258 (2012).
13. A. García-Etxarri, R. Gómez-Medina, L. S. Froufe-Pérez, C. López, L. Chantada, F. Scheffold, J. Aizpurua, M. Nieto-Vesperinas, and J. J. Sáenz, "Strong magnetic response of submicron silicon particles in the infrared," Opt. Express **19**(6), 4815–4826 (2011).
14. M. Nieto-Vesperinas, R. Gómez-Medina, and J. J. Sáenz, "Angle-suppressed scattering and optical forces on submicrometer dielectric particles," J. Opt. Soc. Am. A **28**(1), 54–60 (2011).
15. R. Gómez-Medina, B. García-Cámara, I. Suárez-Lacalle, F. González, F. Moreno, M. Nieto-Vesperinas, and J. J. Sáenz, "Electric and magnetic dipolar response of germanium nanospheres: interference effects, scattering anisotropy, and optical forces," J. Nanophoton. **5**(1), 053512 (2011).
16. A. I. Kuznetsov, A. E. Miroshnichenko, Y. H. Fu, J. Zhang, and B. Luk'yanchuk, "Magnetic light," Sci Rep **2**, 492 (2012).
17. M. Husnik, M. W. Klein, N. Feth, M. König, J. Niegemann, K. Busch, S. Linden, and M. Wegener, "Absolute extinction cross-section of an individual magnetic split-ring resonators," Nat. Photonics **2**(10), 614–617 (2008).
18. R. Gómez-Medina, B. García-Cámara, I. Suárez-Lacalle, L. S. Froufe-Pérez, F. González, F. Moreno, M. Nieto-Vesperinas, and J. J. Sáenz, "Electric and magnetic optical response of dielectric nanospheres: optical forces and scattering Anisotropy," Photon. Nanostruct.: Fundam. Appl. **10**(4), 345–352 (2012).
19. E. D. Palik, *Handbook of Optical Constants of Solid* (Academic, 1985).
20. K. Vynck, D. Felbacq, E. Centeno, A. I. Cãbuz, D. Cassagne, and B. Guizal, "All-dielectric rod-type metamaterials at optical frequencies," Phys. Rev. Lett. **102**(13), 133901 (2009).
21. J. C. Ginn, I. Brener, D. W. Peters, J. R. Wendt, J. O. Stevens, P. F. Hines, L. I. Basilio, L. K. Warne, J. F. Ihlefeld, P. G. Clem, and M. B. Sinclair, "Realizing optical magnetism from dielectric metamaterials," Phys. Rev. Lett. **108**(9), 097402 (2012).
22. C. M. Soukoulis, S. Linden, and M. Wegener, "Physics. Negative refractive index at optical wavelengths," Science **315**(5808), 47–49 (2007).
23. J. B. Pendry, D. Schurig, and D. R. Smith, "Controlling electromagnetic fields," Science **312**(5781), 1780–1782 (2006).
24. X. Chen, Y. Luo, J. Zhang, K. Jiang, J. B. Pendry, and S. Zhang, "Macroscopic invisibility cloaking of visible light," Nat Commun **2**, 176 (2011).
25. B. García-Cámara, F. Moreno, F. González, J. M. Saiz, and G. Videen, "Light scattering resonances in small particles with electric and magnetic properties," J. Opt. Soc. Am. A **25**(2), 327–334 (2008).
26. B. García-Cámara, J. M. Saiz, F. González, and F. Moreno, "Nanoparticles with unconventional scattering properties: size effects," Opt. Commun. **283**(3), 490–496 (2010).
27. B. García-Cámara, F. Moreno, F. González, and O. J. F. Martin, "Light scattering by an array of electric and magnetic nanoparticles," Opt. Express **18**(10), 10001–10015 (2010).
28. B. García-Cámara, J. M. Saiz, F. González, and F. Moreno, "Distance limit of the directionality conditions for the scattering of nanoparticles," Metamaterials (Amst.) **4**(1), 15–23 (2010).
29. M. Kerker, D. S. Wang, and L. Giles, "Electromagnetic scattering by magnetic spheres," J. Opt. Soc. Am. **73**(6), 765–767 (1983).
30. J. M. Geffrin, B. García-Cámara, R. Gómez-Medina, P. Albella, L. S. Froufe-Pérez, C. Eyraud, A. Litman, R. Vaillon, F. González, M. Nieto-Vesperinas, J. J. Sáenz, and F. Moreno, "Magnetic and electric coherence in forward- and back-scattered electromagnetic waves by a single dielectric subwavelength sphere," Nat Commun **3**, 1171 (2012).
31. S. Person, M. Jain, Z. Lapin, J. J. Sáenz, G. Wicks, and L. Novotny, "Demonstration of zero optical backscattering from single nanoparticles," Nano Lett. **13**(4), 1806–1809 (2013).
32. Y. H. Fu, A. I. Kuznetsov, A. E. Miroshnichenko, Y. F. Yu, and B. Luk'yanchuk, "Directional visible light scattering by silicon nanoparticles," Nat Commun **4**, 1527 (2013).
33. B. Brian, B. Sepúlveda, Y. Alaverdyan, L. M. Lechuga, and M. Käll, "Sensitivity enhancement of nanoplasmonic sensors in low refractive index substrates," Opt. Express **17**(3), 2015–2023 (2009).
34. C. Huang, K. Bonroy, G. Reekman, K. Verstreken, L. Lagae, and G. Borghs, "An on-chip localized surface plasmon resonance-based biosensor for label-free monitoring of antigen-antibody reaction," Microelectron. Eng. **86**(12), 2437–2441 (2009).
35. B. Sepúlveda, P. C. Angelomé, L. M. Lechuga, and L. M. Liz-Marzán, "LSPR-based nanobiosensors," Nano Today **4**(3), 244–251 (2009).
36. M. A. Otte, M.-C. Estévez, D. Regatos, L. M. Lechuga, and B. Sepúlveda, "Guiding light in monolayers of sparse and random plasmonic meta-atoms," ACS Nano **5**(11), 9179–9186 (2011).
37. K.-W. Huang, C.-W. Hsieh, H.-C. Kan, M.-L. Hsieh, S. Hsieh, L.-K. Chau, T.-E. Cheng, and W.-T. Lin, "Improved performance of aminopropylsilatrane over aminopropyltriehoxysilane as a linker for nanoparticle-based plasmon resonance sensors," Sens. Act. B **163**(1), 207–215 (2012).
38. L. Guyot, A.-P. Blanchard-Dionne, S. Patskovsky, and M. Meunier, "Integrated silicon-based nanoplasmonic sensor," Opt. Express **19**(10), 9962–9967 (2011).

#189057 - $15.00 USD Received 17 Apr 2013; revised 26 Jun 2013; accepted 31 Jul 2013; published 23 Sep 2013

39. M. Février, P. Gogol, G. Barbillon, A. Aassime, R. Mégy, B. Bartenlian, J.-M. Lourtioz, and B. Dagens, "Integration of short gold nanoparticles chain on SOI waveguide toward compact integrated bio-sensors," Opt. Express **20**(16), 17402–17410 (2012).
40. B. García-Cámara, F. González, F. Moreno, R. Gómez-Medina, J. J. Sáenz, and M. Nieto-Vesperinas, *Smart Nanoparticles Technology,* (InTech, 2012), Chap. 13.
41. C. F. Bohren and D. R. Huffman, eds., *Absorption and Scattering of Light by Small Particles* (John Wiley & Sons, 1983).
42. P. N. Prasad, *Nanophotonics* (John Wiley & Sons, 2004).
43. A. Alù and N. Engheta, "How does zero-forward-scattering in magnetodielectric nanoparticles comply with the optical theorem?" J. Nanophoton. **4**(1), 041590 (2010).
44. B. García-Cámara, F. González, F. Moreno, and J. M. Saiz, "Exception for the zero-forward-scattering theory," J. Opt. Soc. Am. A **25**(11), 2875–2878 (2008).

1. Introduction

The interest of semiconductors photonic microstructures, and in particular silicon photonics, has been demonstrated in the development of several devices, such as waveguides, optical interconnections on chip, lasers, or integrated sensors [1–12]. With the aim of improving their performance and miniaturization capabilities, it has been recently shown that silicon and germanium subwavelength spheres present interesting electric and magnetic Mie resonances [13–16], which could add new functionalities to semiconductor photonics. Semiconductor nanoparticles can behave as photonic nanoresonators due to their high refractive index (*n~3-4*) and to the relationship between the particle size and the incident wavelength [17]. Although the electric dipolar resonance excitation and behavior in high refractive index dielectric nanoparticles is quite similar to that of the localized surface plasmon resonance (LSPR) in metal nanoparticles, the existence of intense magnetic resonances offers new optical features [13,18]. As the optical absorption of several semiconductor materials is substantially lower than that of plasmonic metals [19], some authors has suggested that high refractive index dielectric nanoparticles can be used as the counterpart of metal nanostructures in several applications, as in metamaterials [20,21], to overcome the problems associated to the inherent absorption of plasmonic nanostructures. Additionally, the possibility to excite both electric and magnetic modes can add crucial features to achieve unusual electromagnetic phenomena, such as negative refraction [22], electromagnetic cloaking [23,24], or directionality [26–28]. In this context, it has been recently demonstrated [15] that coherent effects between the electric and the magnetic modes in germanium particles enables control over the scattering direction, as it was predicted by Kerker *et al*. [29] several years ago for hypothetical magneto-dielectric particles. The experimental verification of these predictions has been recently reported in the microwave [30] and visible [31,32] regimes.

In addition to the development of metamaterials, one of the main applications of metal nanostructures has been sensing, due to the high sensitivity of the LSPR to the local changes in the refractive index of the surrounding medium, leading to the development of myriad sensing applications [33–39]. Herein, we have numerically explored the behavior of Mie resonances in high refractive index dielectric nanoparticles as the base of a new generation of optical sensors. We have analyzed the variations of these Mie resonances under changes of the refractive index of the external medium for several particle sizes and semiconductor materials. Finally, we have studied the effect of the external medium on the directionality conditions predicted by Kerker [29,30,40].

2. Methods

The electromagnetic field scattered by a homogeneous and isotropic sphere of radius *a,* illuminated by a linearly polarized plane wave of wavelength λ, can be described via the Lorenz-Mie theory. The scattering and extinction efficiencies of the sphere can be expressed as a multipolar expansion given by [41]:

#189057 - $15.00 USD Received 17 Apr 2013; revised 26 Jun 2013; accepted 31 Jul 2013; published 23 Sep 2013

$$Q_{sca} = \frac{2}{x^2}\sum_{n=1}^{\infty}(2n+1)\left(|a_n|^2 + |b_n|^2\right)$$
$$Q_{ext} = \frac{2}{x^2}\sum_{n=1}^{\infty}(2n+1)\,\mathrm{Re}\left(a_n + b_n\right) \tag{1}$$

where a_n and b_n are, respectively, the electric and magnetic n-polar Mie coefficients, and x is the size parameter defined as $x = k{\cdot}a$, k being the light wavenumber. In addition, the angular distribution of the scattered energy by the sphere is usually described via the differential scattering efficiency [41,42]:

$$Q_{diff} = \frac{1}{x^2}\left\{\left|\sum_n \frac{(2n+1)}{n(n+1)}(a_n\pi_n + b_n\tau_n)\right|^2 + \left|\sum_n \frac{(2n+1)}{n(n+1)}(a_n\tau_n + b_n\pi_n)\right|^2\right\} \tag{2}$$

where τ_n and π_n introduce the angular dependence through Legendre functions of first kind. The particular cases of the differential scattering efficiencies at the forward and backward directions are known as forward scattering (Q_{FS}) and radar backscattering (Q_{RBS}) efficiencies, and are given by [41]:

$$Q_{RBS} = \frac{1}{x^2}\left|\sum_n (2n+1)(-1)^n(a_n - b_n)\right|^2$$
$$Q_{FS} = \frac{1}{x^2}\left|\sum_n (2n+1)(a_n + b_n)\right|^2 \tag{3}$$

For subwavelength particles ($a/\lambda << 1$), as we consider in this work, the multipolar expansion can be well approximated by the sum of the first two electric and magnetic terms (a_1, a_2, b_1 and b_2). Under this approximation, the scattering and extinction efficiencies of the particle are given by:

$$Q_{sca} = \frac{2}{x^2}[3(|a_1|^2 + |b_1|^2) + 5(|a_2|^2 + |b_2|^2)]$$
$$Q_{ext} = \frac{2}{x^2}[3\,\mathrm{Re}(a_1 + b_1) + 5\,\mathrm{Re}(a_2 + b_2)] \tag{4}$$

whereas the differential scattering efficiency is described by:

$$Q_{diff} = \frac{1}{x^2}\left\{\left|\tfrac{3}{2}(a_1 + b_1\cos\theta) + \tfrac{5}{6}(3a_2\cos\theta + 6b_2\cos^2\theta - 3b_2)\right|^2 + \left|\tfrac{3}{2}(a_1\cos\theta + b_1) + \tfrac{5}{6}(6a_2\cos^2\theta - 3a_2 + 3b_2\cos\theta)\right|^2\right\} \tag{5}$$

Finally, the Q_{RBS} and Q_{FS} for such small particle have the following expressions [41,42]:

$$Q_{RBS} = \frac{1}{x^2}\left|-3(a_1 - b_1) + 5(a_2 - b_2)\right|^2$$
$$Q_{FS} = \frac{1}{x^2}\left|3(a_1 + b_1) + 5(a_2 + b_2)\right|^2 \tag{6}$$

Equations (5) and (6) predict that coherent effects can occur between different dipolar and quadrupolar terms in the forward and backward directions. In particular, the electric and the magnetic dipoles can interfere constructively or destructively producing minima in either the backward or the forward scattered intensity at certain light frequencies [13–15]. The relationships between the first two Mie coefficients to achieve the zero-backward or a

#189057 - $15.00 USD Received 17 Apr 2013; revised 26 Jun 2013; accepted 31 Jul 2013; published 23 Sep 2013

minimum forward scattering are denoted as generalized *Kerker's* conditions, and are described as [14,15]:

$$a_1 = b_1,$$
$$\hat{A}(a_1) = -\hat{A}(b_1); \acute{A}(a_1) = \acute{A}(b_1). \tag{7}$$

In the following sections we analyze the evolution of the extinction, differential scattering efficiencies and Kerker's conditions under variations of the external refractive index.

3. Results and discussion

3.1 Spectral analysis of the extinction cross-section

Firstly, we analyze the extinction cross-section of nanospheres with radii (*R*) of *200* and *100 nm*, which are composed of several semiconductor materials whose refractive index ranges from *2.9 to 5*.

Table 1. Semiconductor Materials with High Refractive Index

Material	Refractive index at 1.6 μm	Refractive index at 0.6 μm
AlAs	*2.9 + j0*	*3.17 + j0*
AlSb	*3.28 + j0*	*4.01 + j0.006*
CdTe	*2.73 + j0.25*	*3.01 + j0.36*
GaAs	*3.37 + j0*	*3.91 + j0.22*
GaP	*3.05 + j0*	*3.34 + j0*
Ge	*4.24 + j0*	*5.72 + j1.23*
InP	*3.15 + j0*	*3.56 + j0.33*
PbS	*4.23 + j0.35*	*4.27 + j1.5*
Si	*3.47 + j0*	*3.94 + j0.03*
TiO_2 (rutile)	*2.71 + j0*	*2.93 + j0.04*

Table 1 gathers the refractive index of these materials in the visible and the near-infrared (NIR) [19]. The majority of these materials show small variations in the real part of the refractive index from the visible to the NIR. Only germanium (*Ge*) presents a relative variation of the refractive index larger than 20%. Semiconductors present an important advantage over plasmonic materials: the imaginary part of their refractive index (*k*) is lower, and therefore, their absorption is weaker and most of the light is mainly scattered in nanoparticles. Indeed, Table 1 shows that, with the exception of *CdTe* and *PbS*, *k* is null in the infrared and it weakly increases in the visible, due to the presence of electronic transitions. In the case of *CdTe* and *PbS,* the imaginary part of their refractive index reaches non-negligible values in both visible and NIR regions.

From previous works [13,15,16], we expect that subwavelength particles of these materials present similar spectral behavior as that shown for Si and Ge. Figures 1 and 2 show the extinction efficiency (Q_{ext}) spectra of an isolated sphere of the different semiconductor materials listed in Table 1. To tune the Mie resonances in the NIR or in the visible, we analyze two particle sizes,*R = 200nm* (Fig. 1) and *R = 100nm* (Fig. 2), respectively. In the NIR region, where absorption losses are negligible, most of the particles with *R* = 200 nm present extinction spectra characterized by prominent resonant peaks [Fig. 1]. In the case of *Si, GaP, GaAs, InP, AlSb, AlAs* and *TiO_2*,whos spectra are very similar to each other, the peak at larger wavelengths corresponds to the magnetic dipolar resonance, the central broad peak, which is difficult to observe in *AlAs* and *TiO_2*, is related to the electric dipolar mode, and the sharp peak at shorter wavelengths corresponds to the magnetic quadrupolar mode [13,15,16]. Other less-intense peaks at even shorter wavelengths are due to higher-order multipolar contributions. Although the dipolar contributions in *Ge* also resemble those of previous materials, its higher order multipoles are weak due to the increased absorption at short wavelengths. On the other hand, all resonant peaks blue-shift as the refractive index of the

#189057 - $15.00 USD Received 17 Apr 2013; revised 26 Jun 2013; accepted 31 Jul 2013; published 23 Sep 2013

semiconductor material (n_{sc}) decreases (see Table 1), which is accompanied with an electric dipole peak broadening. Such broadening makes difficult to distinguish the electric dipolar peak for the lowest value of n_{sc}, which correspond to TiO_2.

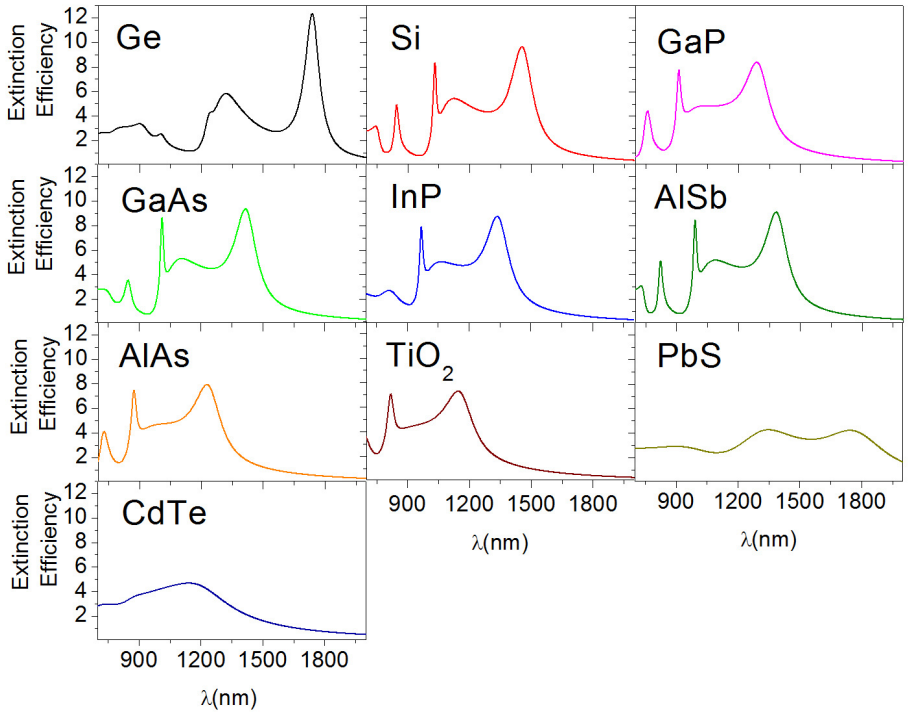

Fig. 1. Extinction efficiency spectra of spherical particles of different semiconductor materials in vacuum ($n_{ext} = 1$). Particle size is $R = 200nm$to achieve Mie resonances in the NIR range.

The exceptions to this general behavior are nanospheres composed of *PbS* and *CdTe*. The non-negligible absorption of these materials in the NIR range generates very broad resonant peaks, thereby limiting the interest of these nanospheres for technological applications.

In contrast, for $R = 100nm$ [Fig. 2], the resonant peaks are in the visible, where the absorption losses are more important. The non-negligible k values in *Ge*, *GaAs* and *InP* result in less intense and broader resonant peaks than those in the infrared. However, the electric and magnetic dipolar modes are still well defined and prominent. On the contrary, *Si*, *AlSb*, *AlAs* and *GaP* have very weak or null absorption in this region, and therefore, their spectra show very intense, well-defined and narrow resonant modes, as in the NIR regime. Nevertheless, the quadrupolar magnetic mode is only barely detected in materials with very low absorption. An example of this behavior is the TiO_2 nanosphere, whose spectrum only shows a well-defined magnetic dipolar peak. Therefore, the higher absorption and the smaller particle size inhibit the excitation of the quadrupolar mode, while the electric dipolar resonance appears as a "shoulder" of the magnetic mode. Likewise larger particles, *CdTe* and *PbS* nanospheres show extinction spectra without well-defined peaks.

#189057 - $15.00 USD Received 17 Apr 2013; revised 26 Jun 2013; accepted 31 Jul 2013; published 23 Sep 2013

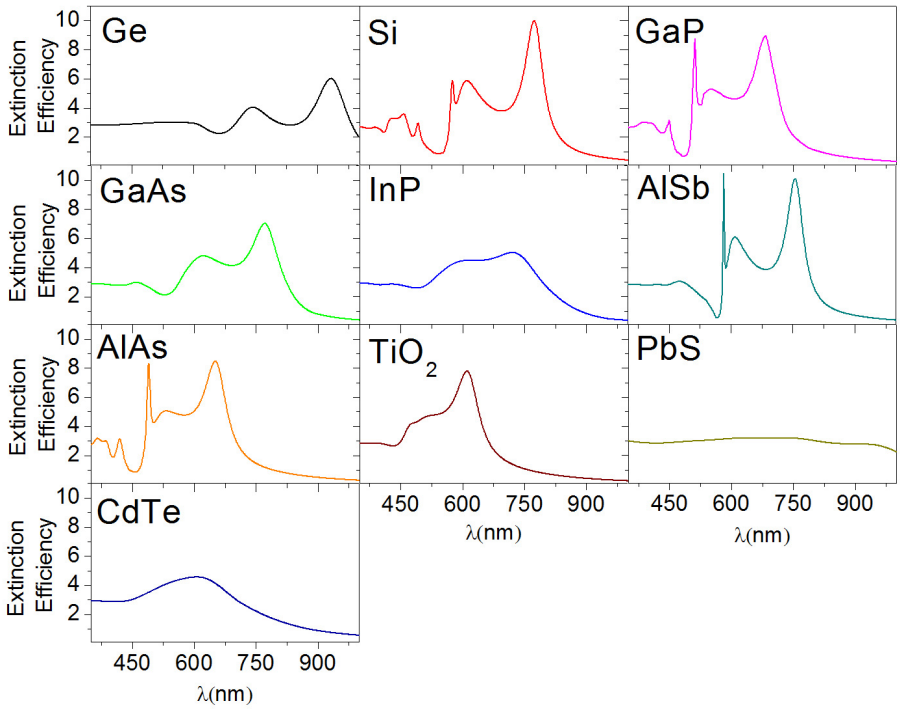

Fig. 2. Extinction efficiency spectra of spherical particles of different semiconductor materials in vacuum (n_{ext} = 1). Particle size is *R = 100nm* to achieve Mie resonances localized in the visible range.

From this analysis, we conclude that semiconductors with values of n_{sc} similar to *Si* or *Ge*, present the expected resonant scattering behaviors [13,15,16]. Furthermore, *CdTe* and *PbS* spectra do not present interesting resonances for practical applications due to their high absorption losses. For that reason, we will not consider them in the following analysis. Interestingly, the magnetic dipolar mode, which appears at larger wavelengths, is the most stable resonant peak, as it is intense and well-defined for most of the materials, and for resonances in the visible and NIR. Consequently, we focus our attention on this mode for the potential sensing applications.

3.2 External refractive index dependence

Nanoplasmonic sensors are typically based on the sensitivity of the LSPR wavelength to the changes in the refractive index of the surrounding medium (n_{ext}) [35,36,42]. Nanoplasmonic sensors commonly detect the shift of the *LSPR* wavelength to monitor in real-time the local changes of refractive index induced by biochemical interactions.

#189057 - $15.00 USD Received 17 Apr 2013; revised 26 Jun 2013; accepted 31 Jul 2013; published 23 Sep 2013

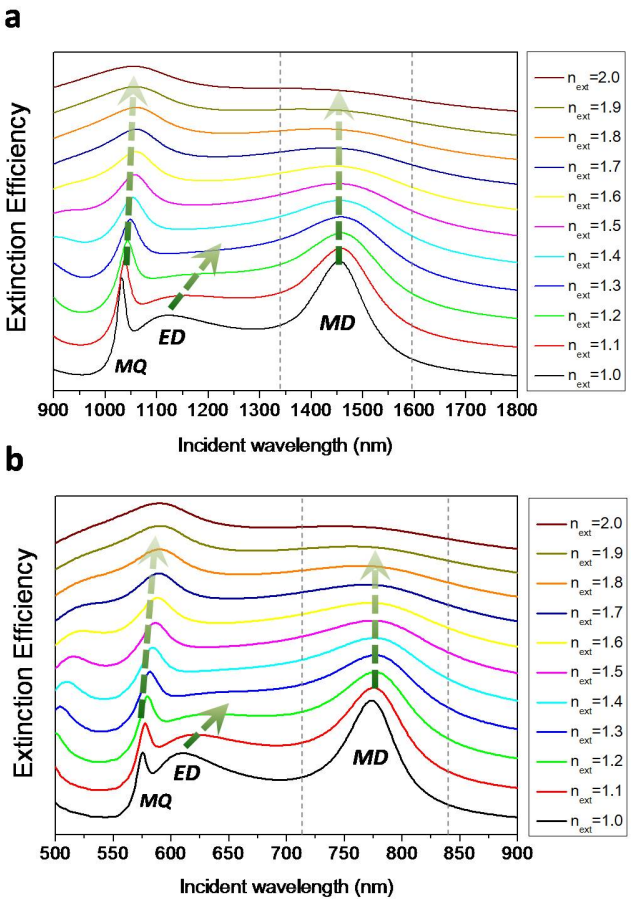

Fig. 3. Extinction efficiency spectra of a spherical silicon particle for several n_{ext} values. Particle sizes are (a) $R = 200nm$ and (b) $R = 100nm$. The three different modes, electric dipolar (ED), magnetic dipolar (MD) and magnetic quadrupolar (MQ), are labeled. Arrows show the evolution of the spectral position of resonances as the external refractive index increases. Vertical lines point the wavelengths that satisfy Kerker's conditions in vacuum. Curves with $n_{ext}>1$ have been shifted upwards (by adding a constant background) for clarity.

In contrast, Fig. 3 shows the variations of Mie resonances in *Si* nanoparticles as a function of n_{ext}, to investigate if this system can be used as refractometric sensing transducer. We consider again two different particles sizes, $R = 200nm$ and $R = 100nm$.The magnetic dipolar mode presents an almost constant spectral position, as it has been recently demonstrated experimentally in silicon colloids [11]. The origin of these phenomena is the localization of the magnetic dipolar mode inside the nanoparticle [13]. The magnetic dipolar peak intensity drastically decreases and broadens as n_{ext} increases. Indeed, for the highest n_{ext} values, the peak is hardly distinguished from the background. The magnetic quadrupolar resonance has a similar behavior, whereas the electric dipolar peak shows a substantial red-shift, but it rapidly broadens and becomes undetectable for $n_{ext}> 1.2$.

#189057 - $15.00 USD Received 17 Apr 2013; revised 26 Jun 2013; accepted 31 Jul 2013; published 23 Sep 2013

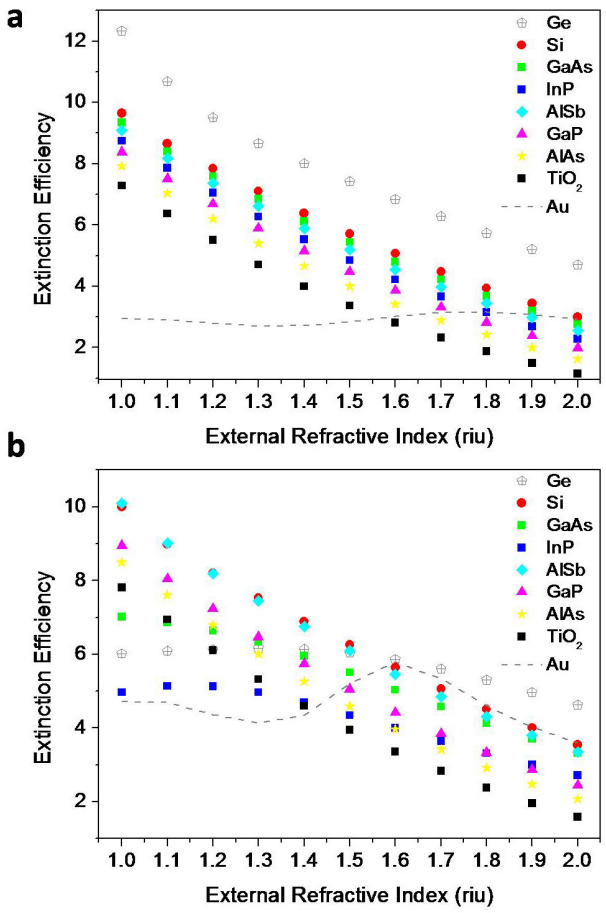

Fig. 4. Extinction efficiency at the magnetic dipolar resonance wavelength in vacuum as a function of the n_{ext}, for nanospheres of different semiconductor materials. The particle sizes are (a) $R = 200nm$ and (b) $R = 100nm$. The evolution of the extinction efficiency of a gold nanosphere at the electric dipolar resonance wavelength is also included as a dashed line.

Interestingly, the drastic drop of the extinction efficiency of the magnetic dipolar resonance as n_{ext} increases could be used as principle of detection for sensing applications. To analyze this potential application, we show in Fig. 4 the extinction efficiency values at the magnetic dipolar resonant wavelength as a function of n_{ext} for nanospheres of the semiconductor materials previously studied, and for two different particle sizes ($R = 200nm$ and $R = 100nm$). As comparison, Fig. 4 also shows the evolution of the extinction efficiency of a gold nanoparticle of the same dimensions, when the wavelength is fixed at the electric dipole resonance wavelength in vacuum. As can be observed, the Q_{ext} evolution of the gold nanoparticle exhibits a complex pattern, which is governed by the redshift of the plasmon electric dipolar and quadrupolar resonances. In contrast, the extinction efficiency of semiconductor nanoparticles at the resonant wavelength of the magnetic dipolar mode in vacuum, decreases monotonously with n_{ext} in most of the materials. The sensitivity to the n_{ext} changes can be calculated *via* the derivative of latter trend:

$$Sensitivity = \frac{\partial Q_{ext}}{\partial n_{ext}}, \tag{12}$$

#189057 - $15.00 USD Received 17 Apr 2013; revised 26 Jun 2013; accepted 31 Jul 2013; published 23 Sep 2013

Figure 5(a) summarizes the sensitivity at n_{ext} = 1.33, which corresponds to the typical background index in biosensing applications. All the materials present similar sensitivities when their magnetic dipolar mode is in the NIR, but there are more drastic variations among materials when this resonance is in the visible. *Ge* and *AlAs* are the most sensitive materials in the NIR and in the visible ranges, respectively, but the values of the sensitivity are comparable. Germanium suffers the most important drop of the sensitivity between NIR and visible ranges as a consequence of the large increase of its absorption in the visible (Table 1).

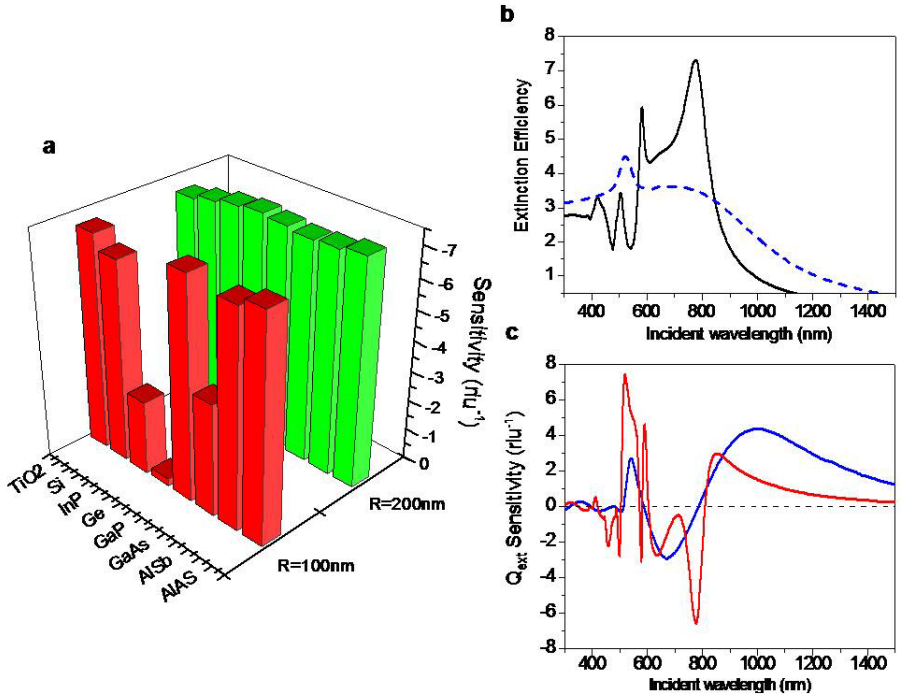

Fig. 5. (a) Sensitivity of the extinction efficiency, at n_{ext} = 1.33, for the considered semiconductor materials and for both particle sizes. (b) Spectral evolution of Q_{ext} in a silicon (solid black line) and in a gold (dashed blue line) nanoparticle of radius $R = 100nm$, embedded in water. (c) Spectral sensitivity of Q_{ext}, at $n_{ext} = 1.33$for a silicon (red curve) and a gold (blue curve) nanoparticle.

Interesting information can be extracted from Figs. 5(b) and 5(c), which compares the spectra of Au and Si nanoparticles when the external medium is water, and their sensitivities to changes of refractive index. Firstly, Fig. 5(b) highlights the substantially higher extinction efficiency of the Si nanoparticle, despite its lower absorption cross section. Additionally, the sensitivity to changes in refractive index displayed in Fig. 5(c) demonstrates the higher sensitivity of the Si nanoparticles and the different spectral behavior. Whereas the maximum sensitivity in Si coincides with the resonant positions of the magnetic dipolar and quadrupolar modes, the maximum sensitivities in Au are observed when the slope of Q_{ext} is maximized, *i.e.* close to the electric dipolar and quadrupolar plasmon resonances. The different behavior is produced by the fact that the magnetic dipolar resonant wavelength of Si is almost insensitive to any change of n_{ext}, while the Au plasmon peak strongly shifts as n_{ext} changes. Overall, the two-fold higher sensitivity expected in the Si nanospheres is accompanied with a 3-fold larger extinction cross section with respect to Au in the most sensitive regions, which can have remarkable implications to improve the limit of detection in refractometric sensors.

#189057 - $15.00 USD Received 17 Apr 2013; revised 26 Jun 2013; accepted 31 Jul 2013; published 23 Sep 2013

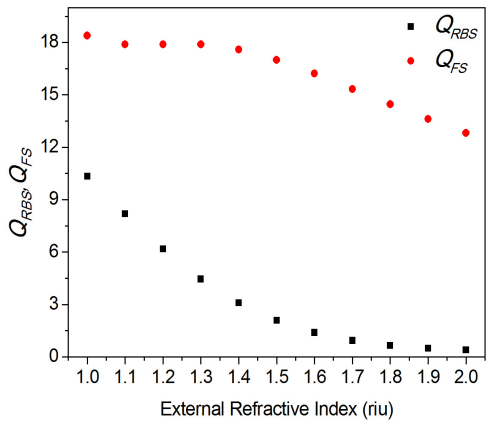

Fig. 6. Forward scattering and radar backward scattering cross sections of a silicon nanoparticle with R = 100nm at the magnetic dipolar resonance wavelength (λ = 773nm).

For actual sensing applications, measurements at the single particle level are not practical due to the generally low signal-to-noise and high background-to-signal ratios of the measurements. An interesting implementation of the presented effects could be achieved via an array of silicon nanospheres with random distribution and mean edge-to-edge separation distance larger than their diameter (equivalent to a surface density of 4-5 nanoparticles/μm^2 for *R = 100 nm* spheres) to simultaneously avoid diffraction and near-field interaction effects [36]. The size of the array could be in the order of 100-500μm^2 to be easily illuminated with low numerical aperture lenses. Since the total extinction efficiency is a complex parameter to be determined experimentally, the experimental detection could be based on the analysis of the forward scattering or radar backscattering cross sections, which can be extracted from extinction measurements either in transmission or in reflection, respectively.

Figure 6 shows both scattering cross sections (Q_{FS}, Q_{RBS}) of a Si nanoparticle (*R = 100 nm*) as a function of the external refractive index at the magnetic dipolar resonance (*λ~773nm*). As can be observed, for n_{ext}< *1.5* the forward scattering remains approximately constant, and the reduction of Q_{ext} mainly comes from the drastic attenuation of the backward scattering efficiency. Consequently, to achieve a high sensitivity in this region, the measurement should be based on the detection of intensity changes in the backscattered light, which in addition will benefit from a low background signal. In contrast, detection of the variations in the forward scattering cross section is the most interesting alternative for n_{ext}> *1.5*, due to the very low backscattering efficiency in this region.

3.3 Radiation pattern variations for sensing

As can be deduced from the previous sections, a very interesting aspect of Mie resonances is related to the ability to control and modify the radiation patterns thanks to the coherent interaction of electric and magnetic dipolar modes, giving rise to zero backward or near-zero-forward scattering radiation patterns [14,15,29,30,43]. In this context, we explore the effect of the external medium on the directionality effects.

#189057 - $15.00 USD Received 17 Apr 2013; revised 26 Jun 2013; accepted 31 Jul 2013; published 23 Sep 2013

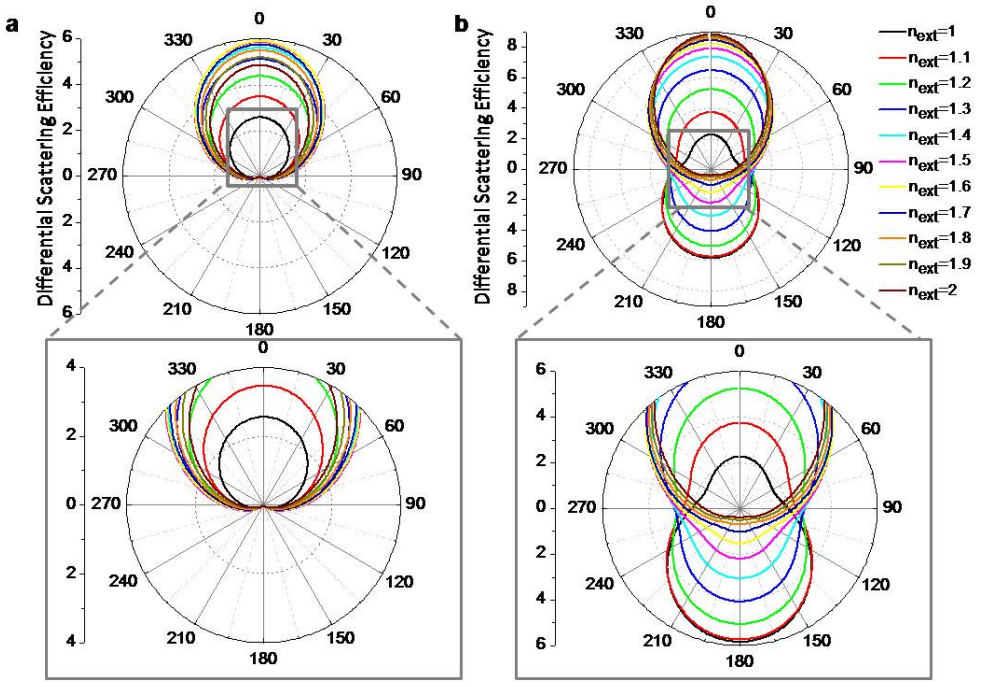

Fig. 7. Polar representation of the differential scattering efficiency, in arbitrary units, of a *Si* nanoparticle *(R = 100nm*) which is illuminated by a plane wave whose wavelength satisfies (a) the zero-backward or (b) the minimum-forward condition in vacuum, for several values n_{ext}. The incident light beam is linearly polarized with the electric field perpendicular to the scattering plane. A zoom of the central area is shown in the bottom part of the figure to observe in detail the evolution as n_{ext} changes.

Figure 7 shows the variation of the differential scattering efficiency of a *Si* nanoparticle of *R = 100nm* at the incident wavelengths that satisfy Kerker's conditions in vacuum (*i.e.* λ = *843.6nm* for the first Kerker's condition or zero-backward scattering, and λ = *717.8nm* for the second condition or near-zero-forward scattering) when n_{ext} increases. To observe the changes in detail, we also plot a zoom of the polar plots in the bottom part. As can be seen, while the zero-backward condition can be kept for any value of the external refractive index, the minimum forward condition is very sensitive to n_{ext}. In fact, although the extinction cross section does not significantly change as n_{ext} increases, there is rapid transformation of the radiation pattern from near zero forward to near zero backward. Such effect is a consequence of the red-shift of the electric dipolar resonance that also modifies the wavelength at which the second condition is satisfied. For practical applications, detection of the forward scattering and radar backscattering efficiencies can be an interesting alternative. Figure 8 plots the evolutions of these parameter with n_{ext}, showing that the forward scattering linearly increases for n_{ext}<*1.4*, whereas the radar backscattering shows a region with high sensitivity to refractive index changes for n_{ext} comprised between *1.2* and *1.6*. Therefore, analysis of the forward or backward scattering of an arrays of subwavelength dielectric particles illuminated by a light beam whose wavelength satisfies Kerker's condition in vacuum, can also be used as a new sensing principle of detection. This effect clearly shows potential experimental benefits, since this measurement could be experimentally performed by simply detecting extinction variations in transmission or reflection at a fixed wavelength, in an array of silicon nanospheres similar to that previously described.

#189057 - $15.00 USD Received 17 Apr 2013; revised 26 Jun 2013; accepted 31 Jul 2013; published 23 Sep 2013

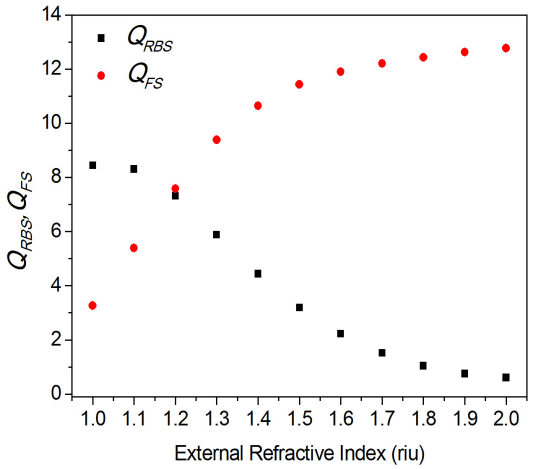

Fig. 8. Forward scattering and radar backscattering efficiencies, at the wavelength that satisfies Kerker's condition of minimum forward scattering in vacuum for a Si nanoparticle (R = *100nm*) as a function of the external refractive index

4. Conclusions

We have investigated the spectral and radiation pattern responses of Mie resonances in subwavelength semiconductor spherical particles under changes of the external refractive index. We have shown that the behavior of the magnetic dipolar resonance has remarkable potential sensing applications in two different configurations. The first configuration exploits the strong reduction of the extinction cross-section peak associated to the magnetic dipolar resonance as n_{ext} increases. When the resonance is in the NIR, the most sensitive material is *Ge* due to its very high refractive index and negligible losses, whereas the highest sensitivities in the visible are achieved by *Si* and *AlSb*, as a consequence of the general increase of the absorption in all semiconductor material. The second configuration is based on the variation of the directionality of the scattered radiation at the Kerker's conditions. While zero-backward scattering condition is very stable and does not vary as n_{ext} changes, the minimum-forward condition shows a fast conversion from near zero forward to near zero backward scattering as the refractive index of the external medium increases. Thus, the change in the scattering radiation pattern could also be used as a new sensing parameter, *via* analysis of the forward scattering or radar backscattering efficiencies.

The use of these parameters could involve important advantages with respect to conventional plasmon sensors. Firstly, the drastic reduction of the absorption losses with respect to the plasmonic nanostructures eliminates the problems and risks associated to plasmonic heating at moderate or high light intensity. This feature can be crucial to ensure the stability of biomolecules or even live cells, while enabling the use of high intensity to improve the signal-to-noise ratio (SNR) of the measurements. Secondly, nanoplasmonic sensors typically monitor the LSPR wavelength shifts induced by the local changes of refractive index generated by biochemical interactions. A high signal-to-noise ratio involves the necessity of spectrometers with high spectral resolutions along a large wavelength range, in which the time resolution is in the millisecond range.In contrast, our proposal only needs the detection of the intensity variations at the magnetic dipolar resonance or at the Kerker's condition wavelength, thus reducing technological requirements and costs, and opening the path to ultra-fast detection, which is especially interesting for single molecule detection applications.

#189057 - $15.00 USD Received 17 Apr 2013; revised 26 Jun 2013; accepted 31 Jul 2013; published 23 Sep 2013

Acknowledgments

B.G.-C. acknowledges support from the JAE-Doc program of the Spanish Council of Research (CSIC). This research has been funded by Ministerio de Ciencia e Innovación, through grants: Consolider NanoLight (CSD2007-00046), FIS2009-13430-C02, as well as by the Comunidad de Madrid (Microseres-CM, S2009/TIC-1476)

#189057 - $15.00 USD Received 17 Apr 2013; revised 26 Jun 2013; accepted 31 Jul 2013; published 23 Sep 2013